Physics of the Solid State, 2024, Vol. 66, No. 11

05,10

Synthesis of textured barium hexaferrite films on silicon substrates with amorphous $Al_2O_3|Si_3N_4$ coating

© V.G. Kostishyn[1], A.Yu. Mironovich[1,¶], A.V. Timofeev[1], G.A. Skorlupin[1], A.I. Ril[2]

[1] Federal State Autonomous Educational Institution of Higher Education
≪National Research Technological University „MISIS"≫
Moscow, Russia
[2] Federal State Budgetary Institution of Science
„Kurnakov Institute of General and Inorganic Chemistry of the Russian Academy of Sciences",
Moscow, Russia
¶ E-mail: mironovich.ai@misis.ru

Received October 30, 2024
Revised November 2, 2024
Accepted November 3, 2024

$BaFe_{12}O_{19}$ thin films were synthesized by ion-beam sputtering on amorphous $Al_2O_3|Si_3N_4$ structures. Immediately after sputtering, the $BaFe_{12}O_{19}$ films are amorphous, but can be converted to a crystalline state by annealing. In this case, under certain conditions, a $(00l)$ texture spontaneously forms in such films, which allows them to be used for designing and creating planar microwave devices, spintronics and magnetic memory devices. However, due to heat treatment, mechanical stresses arise in the $BaFe_{12}O_{19}|Al_2O_3|Si_3N_4$ structure, leading to the formation of macroscopic defects. In this work, we study the possibility of reducing stresses by additional annealing of the Al_2O_3 and Si_3N_4 layers at 900°C and varying the Al_2O_3 thickness in order to obtain defect-free $BaFe_{12}O_{19}$ $(00l)$ films.

Keywords: Hexagonal ferrite, Thin films, Surface morphology, Ion-beam deposition, Crystallographic texture.

DOI: 10.61011/PSS.2024.11.60094.290

1. Introduction

M-type barium hexaferrite (BaM) is a complex oxide with the stoichiometric formula $BaFe_{12}O_{19}$ or $BaO \cdot 6Fe_2O_3$ and a structure isomorphic to the magnetoplumbite of the space group $P6_3/mmc$ [1]. This material has been widely used in various fields of technology since 1952, when the Dutch company Philips introduced it into production under the name ferroxdure [2]. The wide practical application of BaM is attributable to the unique set of properties and characteristics of this compound: anisotropy field $H_a \approx 16$ kOe [3,4], coercive force $H_c = 920-4600$ Oe, saturation magnetization $M_s = 4.4$ kG [5,6], ferromagnetic resonance line frequency and width $f_{\text{FMR}} \approx 40-60$ GHz and $\Delta H \approx 130-210$ Oe, respectively [7], Curie temperature $\sim 497°$C [8]. Studies of this material remains relevant at the present time despite the long history of the use of barium hexaferrite. Thus, the trend towards miniaturization of devices observed in electronics has not pass by BaM. Anisotropic BaM films can be the basis for creating planar microwave devices [9]: circulators [10], insulators [11] and phase shifters [12]. One of the main requirements for such films is the presence of strong magnetic anisotropy, which is more pronounced the higher the degree of crystallographic texture of the hexaferrite.

The following methods are usually used to produce hexaferrite films: liquid-phase epitaxy [13], vacuum sputtering [5,14,15], screen printing [16,17] and the sol-gel method [18,19]. The main advantage of liquid-phase epitaxy is the possibility of obtaining single-crystal films of BaM [13], however, the use of platinum accessories (crucible, agitator, substrate holder) and high-quality single-crystal substrates significantly increases the final cost of the material. These obstacles slow down both the entry of devices to the market and studies. On the other hand, films obtained by more accessible synthesis methods, such as the sol-gel method [18,19] or chemical deposition from solution [20], are characterized by a low degree of texture and, as a result, weak magnetic anisotropy compared to films obtained by other methods. Films obtained by vacuum methods have an acceptable price–quality ratio and can be used as a seed layer in liquid-phase epitaxy [21]. On the other hand, the production of textured BaM films is a challenging task because of the material's significant sensitivity to the parameters of the process [22].

The choice of substrate plays an important role in the synthesis of anisotropic films regardless of the production technology used. Monocrystalline sapphire plates are most widely used, ensuring the growth of c-oriented ferrite films because of the similarity of the oxygen planes of Al_2O_3 (001) and BaM (001) [23]. $Pt(111)|SiO_2|Si$ configuration is also often used for the synthesis of hexaferrite films because of the compatibility of dense packages of Pt(111) and BaM(001). This structure is more accessible and easier to manufacture than sapphire due to the spontaneous textured growth of platinum on amorphous substrates [24], which is attributable to the lowest energy of nuclei with orientation (111) in FCC-metals [25]. Spontaneous texturing is also typical for materials with HCP, so that barium hexaferrite films with texture $(00l)$ can be grown on amorphous substrates [26,27]. However, the widely used amorphous silicon dioxide is apparently not suitable for the synthesis of high-quality anisotropic BaM films [28]. High-temperature annealing of hexaferrite is accompanied by the diffusion of silicon from the substrate [29], which affects the orientation of the resulting grains [30]. Nevertheless, the successful growth of textured hexaferrite was demonstrated on amorphous films of $AlO(10\,nm)|Si_3N_4$ [27] and $AlO(10\,nm)|SiO_2$ [31]. It was also shown that the sublayer material affected the characteristics of BaM despite the contact of BaM with AlO. $AlO|Si_3N_4$ structure was characterized as more advantageous for further deposition and growth of the anisotropic BaM film, because of the incomparably high thermal stability of Si_3N_4 compared to SiO_2. Nevertheless, the chemical inertia of the substrate alone is not sufficient for producing films suitable for practical use. Silicon wafers with amorphous Al_2O_3, Si_3N_4 and combinations thereof were used as substrates in another study [32]. The hexaferrite film grown on $Si_3N_4|Si$ substrate was of unsatisfactory quality because of the presence of macroscopic defects. The mechanical stresses that occur during the formation of the nitride layer and subsequent high-temperature treatment led to the formation of blisters, which is quite often observed in the presence of significant compressive stresses in films [33]. The thicker the layer of Si_3N_4, the higher the mechanical stresses, which resulted in an increase of the average defect radius. An additional layer of Al_2O_3 made it possible to reduce the stress and obtain a BaM film without blisters. Silicon nitride, which has high thermal stability, acts as a diffusion barrier in the structure of $Al_2O_3|Si_3N_4|Si$, and aluminum oxide compensates for the stresses occurring in the nitride. In general, the spontaneous formation of BaM with an c-axis perpendicular to the plate plane was confirmed, which demonstrates the promising outlooks of composition of $Al_2O_3|Si_3N_4|Si$. For this reason it is advisable to conduct further studies of this material. In particular, the possibility of stress modulation for obtaining a defect-free film is the most relevant issue. This paper considers the possibility of synthesizing $BaM\,(00l)|Al_2O_3|Si_3N_4|Si$ films without macroscopic defects by reducing stresses by heat treatment and adjusting the thickness of aluminum oxide.

2. Experimental part

Experimental samples of $BaM|Al_2O_3|Si_3N_4|Si$ films were obtained by ion-beam sputtering and plasma chemical deposition from the gas phase followed by annealing in an air furnace. First, silicon wafers with orientation (111) were washed in isopropyl alcohol (80°C, 180 s), deionized water (30 s) and dried in atmosphere of N_2 for 250 s at 70°C. Silicon nitride with a thickness of 100 nm was deposited on a Si substrate by plasma chemical deposition using Corial D250 system. The substrate deposition temperature, operating pressure, and RF generator power were 250°C, 2000 mTorr, and 90 W, respectively. A mixture of SiH_4, NH_4, N_2 and Ar with a flow rate of 50, 180, 1500 and 100 cm^3/min, respectively, was used as the working atmosphere. BaM and Al_2O_3 films were deposited by ion-beam sputtering using the UVN-71 system. $Si|Si_3N_4$ substrates were additionally cleaned in an ultrasonic bath with isopropyl alcohol before deposition. The substrate holder was positioned opposite the target at a distance of 36 mm. The discharge current, discharge voltage, and operating pressure(Ar) during the process were maintained at 40 mA, 2 kW, and $3 \cdot 10^{-4}$ Torr, respectively. The temperature of the substrates during deposition was 300−330°C. The samples were produced in 4 routes, which are shown in Figure 1. Each route contains three samples with different thicknesses of Al_2O_3 (50, 100 and 200 nm). The thickness of BaM is about 90 nm in all cases. Route IV also included a BaM deposition stage, but the experiment was interrupted, which will be explained in the next section.

The obtained films were studied by several methods, X-ray diffraction (XRD), atomic force microscopy (AFM), and contact profilometry. X-ray diffraction patterns were obtained in the Centre of Shared Equipment of IGIC RAS using Bruker D8 Advance diffractometer (radiation CuK_α, $\lambda = 0.154$ nm, $U = 40$ kV, $I = 40$ mA). Match!3 software environment was used to process diffraction patterns. Atomic force microscopy micrographs and optical images of the surface were obtained using NT-MDT NTEGRA Prima scanning probe microscope. The thickness of the films was checked using DekTak 150 contact profilometer with an error of no more than 5.6%.

3. Results and discussion

It is advisable to start with the systematization of samples for the convenience of the description. A specific code was assigned to each sample. For example, one of the samples is named „A−N−50", where the first letter indicates the heat treatment of Si_3N_4 layer, „A" — „annealed"; the second letter indicates the heat treatment of Al_2O_3 film, „N" — „not annealed"; and the number indicates the thickness of aluminum oxide, expressed in nanometers.

First, the surface of aluminum oxide was analyzed on all samples using optical microscopy. Typical macrodefects caused by stresses in films were found only in samples with type A−A (Figure 2). The evolution of defects with the increase of thickness of Al_2O_3 can be seen in these films, starting from relatively small dots (Figure 2, a) turning into a network of cracks (Figure 2, c). Cracks are usually observed in films with tensile stress, unlike round blisters caused by strong compressive stress [34]. The observation of cracks in this context (Figure 2, c and d) confirms that Al_2O_3 film is under tensile stress (at least after reaching an alumina thickness of 200 nm). Moreover, this stress is significantly enhanced or even induced by annealing, since samples of type A−N and N−N had no visible defects in Al_2O_3 layer. Also, no large defects were found in N−A films. This

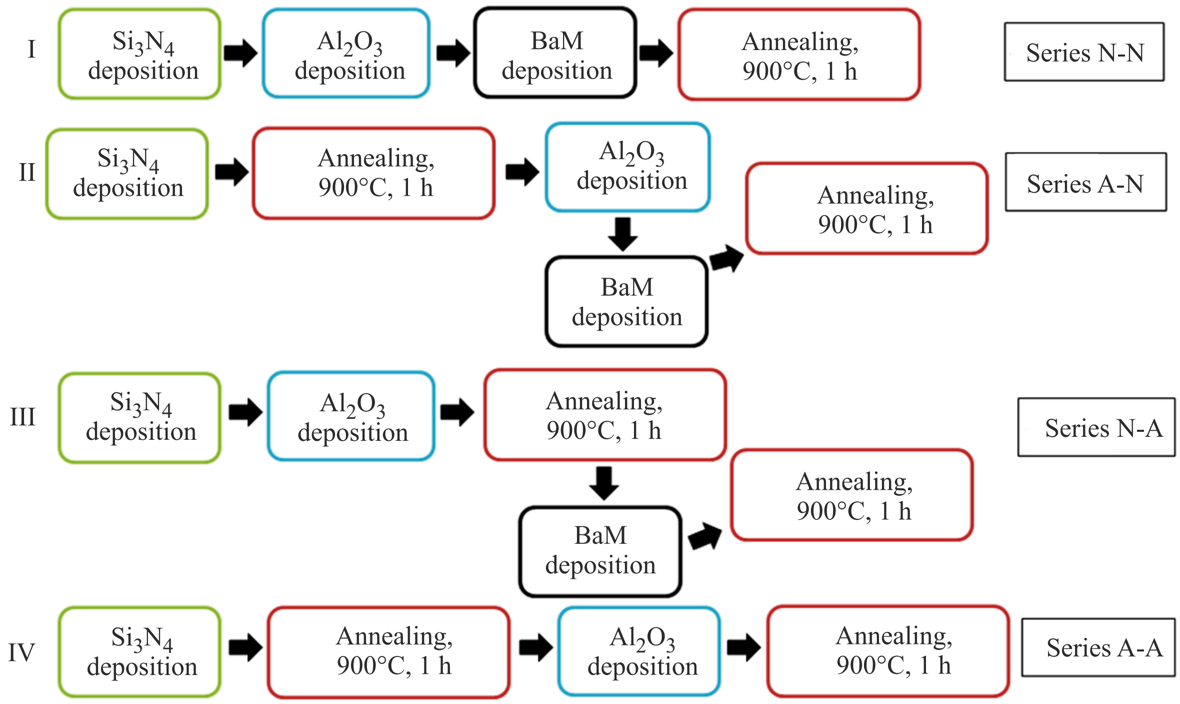

Figure 1. Schemes for the production of experimental samples.

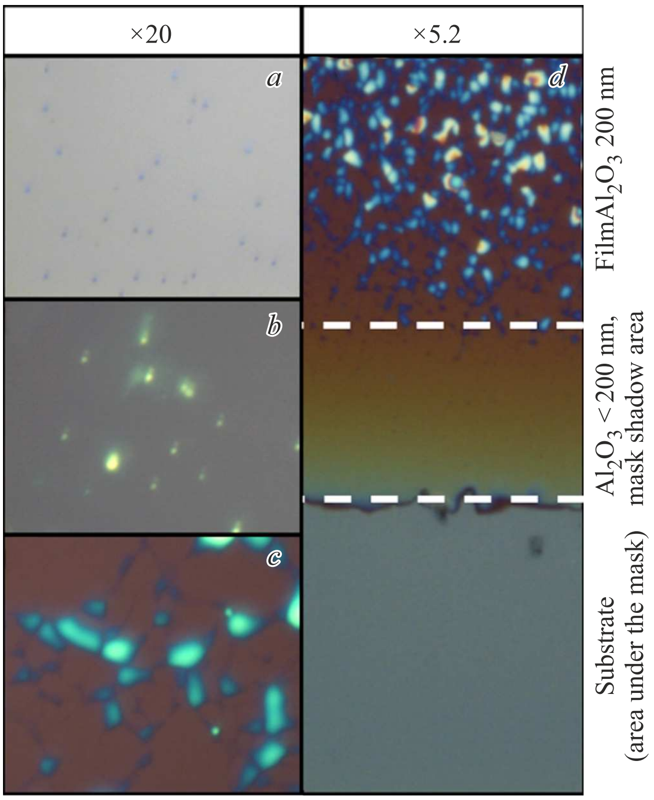

Figure 2. Photographs of the surface of annealed films of Al_2O_3 with thickness *a*) 50 nm, *b*) 100 nm and *c*) 200 nm deposited on annealed Si_3N_4 (series of samples A–A); *d*) image of the area near the edge of the film, additionally illustrating the dependence of stresses on the thickness of Al_2O_3.

can be interpreted as the annealing of Si_3N_4 reduces the compressive stresses in this layer. Thus, the absence of defects in A–N, N–A and N–N series is attributable to compensation of tensile stresses in aluminum oxide and compressive stresses in silicon nitride. Defects appear in the structure when the balance is significantly disrupted, as in samples A–A, where the compressive stresses in Si_3N_4 are reduced, and on the contrary, the tensile stresses in Al_2O_3 are increased due to annealing.

An experiment was also conducted to deposit BaM onto the annealed silicon nitride without an intermediate layer of Al_2O_3 taking into account the stress reduction in Si_3N_4 due to temperature treatment. Many blisters were found on the film surface after its annealing (Figure 3, *a*).

Since Al_2O_3 coating is defective in samples of type A–A, then further sputtering of BaM is impractical, and no subsequent experiments have been conducted for this series. Most of the other samples were defective after BaM annealing, except for the cases of A–N–200 and N–N–200. Considering this result, as well as the analysis of the BaM|Si_3N_4 film (annealed), it can be assumed that the intrinsic compressive stresses in BaM, caused by a decrease of the volume of the film during its crystallization from the amorphous state, contribute to the formation of blisters in the structure of BaM|Al_2O_3|Si_3N_4. Thus, the thicker the aluminum oxide film and the greater the tensile stresses caused by it, the fewer blisters will be observed until a stress equilibrium is reached and the defects disappear altogether. Nevertheless, annealing of Si_3N_4 leads to a slight decrease of the concentration of blisters, as can be seen from samples with the same thickness of Al_2O_3

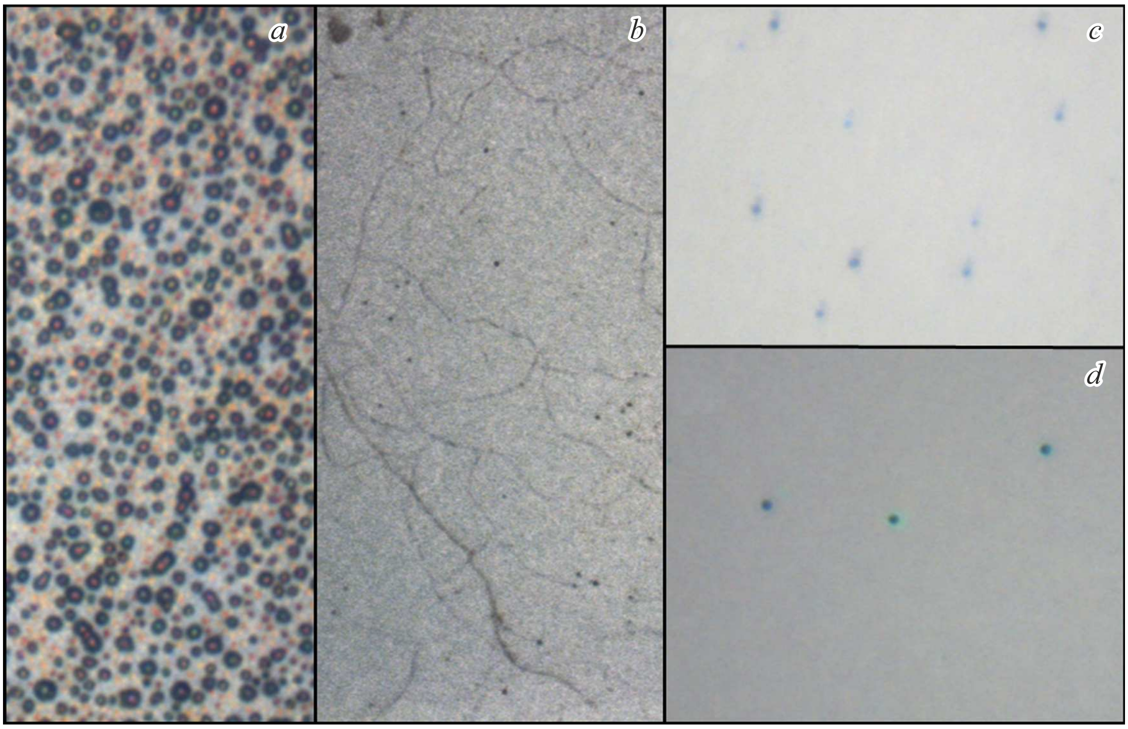

Figure 3. Photographs of annealed BaM films on *a*) annealed Si_3N_4, *b*) $Al_2O_3|Si_3N_4$: N–A–200, *c*) N–N–100, *d*) A–N–100. Magnification ×20.

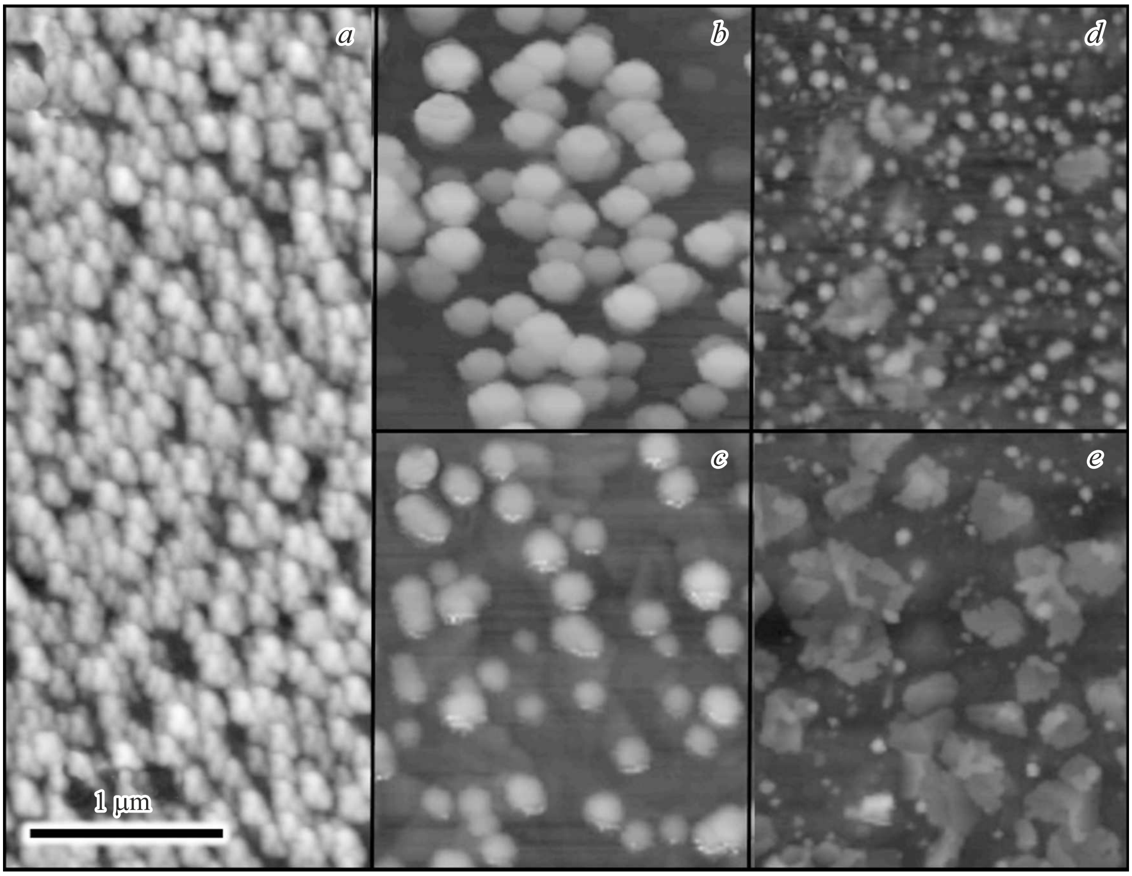

Figure 4. AFM micrographs of samples $BaM|Al_2O_3|Si_3N_4$: *a*) N–N–100, *b*) N–N–200, *c*) N–A–50, *d*) N–A–200, *e*) A–N–50.

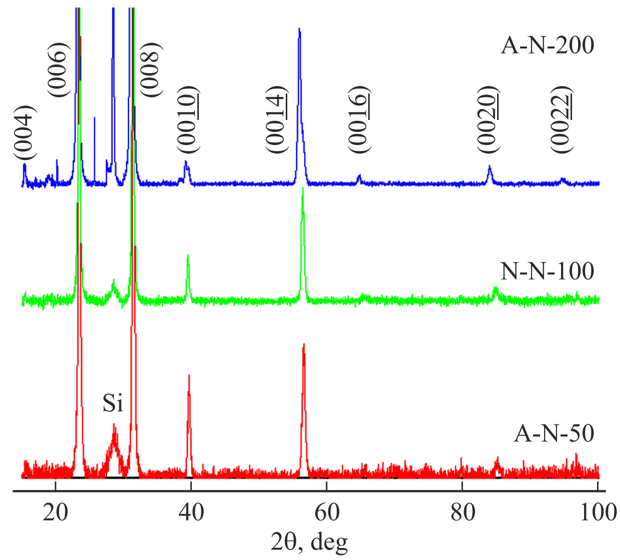

Figure 5. X-ray diffraction patterns of A−N−50, N−N−100 and A−N−200 films. The diffraction pattern was recorded after thickening of BaM by deposition of additional layers for the sample of A−N−200. Hexaferrite peaks were identified using the card COD № 1008328.

(Figure 3, *c* and *d*). A further increase of tensile stresses, either due to thickening or annealing of Al_2O_3, should initiate a change of the type of defects from blisters to cracks. This effect was observed in N−A−200 films, in which the BaM film is covered with cracks rather than blisters, as in the other samples (Figure 3, *b*). The maximum tensile stresses possible under the conditions of this experiment occur in BaM|Al_2O_3|Si_3N_4 structure during the synthesis of N−A−200 which is attributable to annealing and the largest thickness of Al_2O_3.

The synthesized hexaferrite films also differ markedly in microstructure. Nevertheless, the films obtained mainly consist of rounded grains characteristic of the texture $(00l)$ BaM. The crystallites have slightly oval shape, low relief heterogeneity and are densely packed in samples of N−N−50, N−N−100 and A−N−200 (Figure 4, *a*). Sample of N−N−200 is characterized by the presence of separate clusters of grains on the surface, which leads to increased roughness (Figure 4, *b*). A similar microstructure with a more sparse arrangement of grains on the surface is observed in samples of N−A−50 and N−A−100 (Figure 4, *c*). Inclusions of needle-like grains were observed in A−N−100 films, which negatively affects the degree of texture and, consequently, magnetic anisotropy. Large irregular protruding structures are observed on the surface of samples of N−A−200 and A−N−50 in addition to rounded grains. Similar structures are known by the term „hillocks" and are formed in thin films as a product of stress relaxation. A similar microstructure was previously observed in BaM(001)|Al_2O_3(102) films, where these elements provided stress relaxation of the nonconformity between the film and substrate structures [35].

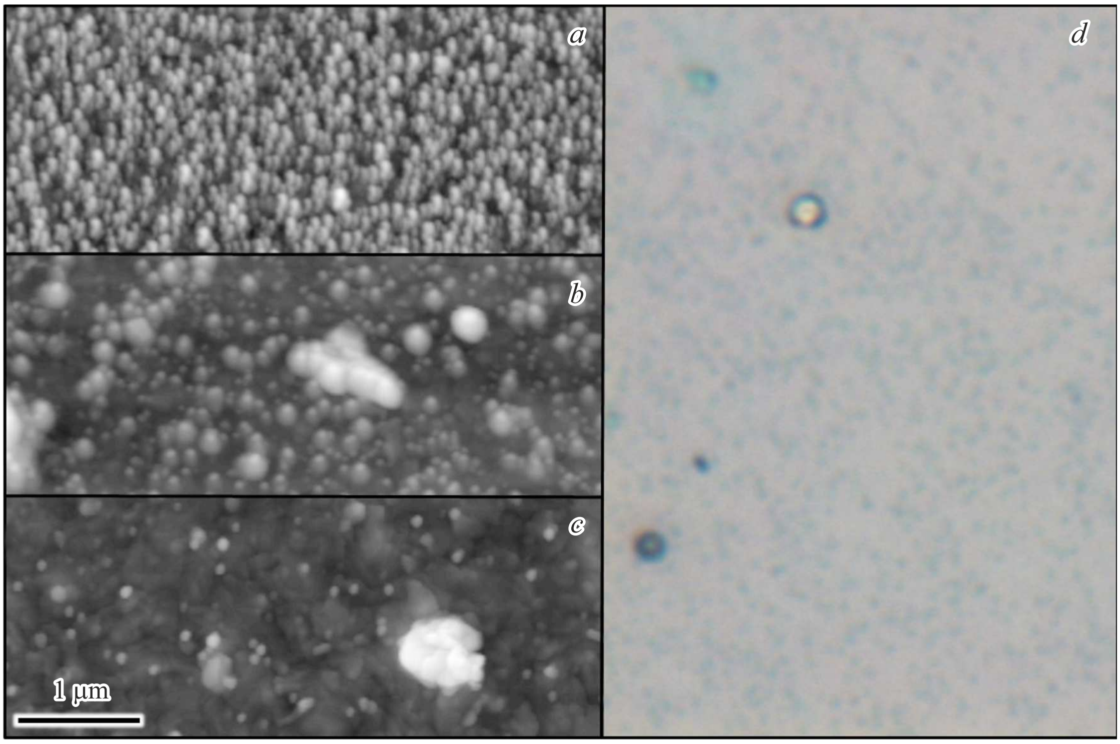

Figure 6. AFM micrographs of A−N−200 film after deposition and annealing additional layers of BaM: *a*) the first (initial) layer, *b*) the second layer, *c*) the third layer. *d*) Optical photograph of the surface of the third layer, ×20 magnification.

Despite the differences of the microstructure of the films, their X-ray diffraction patterns are conceptually the same and reflect the presence of hexaferrite with a texture $(00l)$ (for example, samples of N−N−100 and A−N−50 (Figure 5).

The highest quality A−N−200 film with a defect-free surface and homogeneous microstructure was used in further experiments to determine the possibility of synthesizing thicker BaM films on the structure $Al_2O_3|Si_3N_4$. The procedure of sequential deposition of additional layers of barium hexaferrite followed by annealing was applied for this purpose [36]. The thickness of each new layer was about 100 nm, and the annealing temperature was 900°C. This approach is attributable to the fact that the known methods of increasing the thickness are less reliable in terms of maintaining a high degree of texture $(00l)$. Thus, a simple increase of the deposition time will lead to a thickening of the initial amorphous BaM film, but non-oriented crystallites will form in it after crystallization annealing [37].

The evolution of the microstructure of the BaM film in sample A−N−200 with an increasing number of deposition-annealing iterations is shown in Figure 6. It can be seen that the round shape of the grains and, as a result, their orientation did not change with the film growth. However, the initial uniformity of grain sizes was lost (Figure 6). There are structures, similar to hillocks in samples N−A−200, A−N−50 and in films in [35], which can be considered as a sign of an increase of stresses in the structure. Defects characteristic of samples with uncompensated compressive stresses also occur on the surface of the film.

At the same time the predominant orientation of hexaferrite $(00l)$ remains after increasing the film thickness according to X-ray diffraction patterns (Figure 5). However, some additional peaks appear at 19, 20.5, and 25.5°, which can be interpreted as follows. Firstly, the grains that make up the blisters observed on the surface should definitely have an orientation different from the „intact" part of the film. The peak at 19° can be attributed to this grain fraction, since it corresponds to the position of the barium hexaferrite reflex (012), and also correlates in shape with other BaM peaks. Secondly, local destruction of the hexaferrite film (for example, in case of rupture of a blister) can lead to exposure of the surface of the Si substrate. In this case, silicon will oxidize upon contact with the atmosphere during the thermal treatment of the sample. Thus, the narrow reflexes at 20.5 and 25.5° can be attributed to silicon oxide formed under synthesis conditions as a side phase. This interpretation is supported by diffraction patterns obtained earlier on silicon substrates oxidized at 900°C, on which these reflections were also recorded [38].

4. Conclusion

Thin films of textured barium hexaferrite were produced by ion-beam sputtering on the amorphous structure $Al_2O_3|Si_3N_4|Si(111)$. The effect of pre-annealing of layers of Al_2O_3 and Si_3N_4 and the thickness of Al_2O_3 on the defect and the microstructure of barium hexaferrite films was studied. It can be concluded according to the study of the film surface that heat treatment leads to an increase of tensile stresses in Al_2O_3 and a decrease of compressive stresses in Si_3N_4. In this case, compressive stresses occur directly in the BaM film as a result of crystallization annealing. It is shown that the stresses can be compensated by changing the synthesis conditions such as the presence of thermal treatment of Al_2O_3 and Si_3N_4 and the thickness of the layer of Al_2O_3 and a barium hexaferrite film can be obtained without macroscopic defects. In addition, the impact of these factors on the microstructure of BaM has been demonstrated. In particular, barium hexaferrite films with morphologically homogeneous nanometer-scale grains were obtained. At the same time, the obtained BaM films have a texture of the type $(00l)$ according to the results of X-ray phase analysis, which makes possible their practical application in such fields as magnetic memory and spintronics.

Funding

The study was supported by a grant from the Russian Science Foundation (project No. 24-13-00268).

Conflict of interest

The authors declare that they have no conflict of interest

References

[1] R.C. Pullar. Prog. Mater. Sci. **57**, *7*, 1191 (2012).
[2] J.J. Went, G.W. Rathenau, E.W. Gorter, G.W. van Oosterhout. Philips Techn. Rev. **13**, *7*, 194 (1952).
[3] D. Chen, G. Wang, Z. Chen, Y. Chen, Y. Li, Y. Liu. Mater. Lett. **189**, 229 (2017).
[4] H. Zheng, J. Luo, Q. Wu, P. Zheng, L. Zheng, M. Han, Y. Zhang. J. Magn. Magn. Mater. **479**, 99 (2019).
[5] C. Yu, A.S. Sokolov, P. Kulik, V.G. Harris. J. Alloys. Compd. **814**, 152301 (2020).
[6] S.D. Johnson, D.-S. Park, S.B. Qadri, E.P. Gorzkowski. J. Magn. Magn. Mater. **479**, 156 (2019).
[7] X. Dong, H. Li, J. Chen, D. Chen, J. Shen, Y. Chen. Mater. Res. Express **6**, *9*, 096104 (2019).
[8] S. Mahadevan, C. Pahwa, S.B. Narang, P. Sharma. J. Magn. Magn. Mater. **441**, 465 (2017).
[9] V.G. Harris, A. Geiler, Y. Chen, S.D. Yoon, M. Wu, A. Yang, Z. Chen, P. He, P.V. Parimi, X. Zuo, C.E. Patton, M. Abe, O. Acher, C. Vittoria. J. Magn. Magn. Mater. **321**, *14*, 2035 (2009).
[10] R. Bowrothu, H.-I. Kim, C.S. Smith, D.P. Arnold, Y.-K. Yoon. IEEE Trans. Microw. Theory Tech. **68**, *12*, 5065 (2020).
[11] W.M. Gitzel, O. Arikan, M. Heidenreich, J. Töpfer, A.F. Jacob. 2020 50th Eur. Microw. Conf. 739 (2021).
[12] Z. Wang, Y.-Y. Song, Y. Sun, J. Bevivino, M. Wu, V. Veerakumar, T.J. Fal, R.E. Camley. Appl. Phys. Lett. **97**, *7*, 72509 (2010).
[13] S.G. Wang, S.D. Yoon, C. Vittoria. J. Appl. Phys. **92**, *11*, 6728 (2002).

[14] K. Sun, Q. Li, H. Guo, Y. Yang, Z. Yu, Z. Xu, X. Jiang, Z. Lan, L. Li. J. Alloys Compd. **663**, 645 (2016).
[15] A.R. Abuzir, S.A. Salman, J. Mazher. J. Supercond. Nov. Magn. **33**, *12*, 3819 (2020).
[16] N. Velhal, G. Kulkarni, D. Mahadik, P. Chowdhury, H. Barshilia, V. Puri. J. Alloys Compd. **682**, 730 (2016).
[17] Y. Chen, T. Sakai, T. Chen, S.D. Yoon, A.L. Geiler, C. Vittoria, V.G. Harris. Appl. Phys. Lett. **88**, *6*, 062516 (2006).
[18] F.K.H. Gellersen, F.M. Klichowski, A.G.C. Rusche, A.F. Jacob. 2016 Ger. Microw. Conf. 221 (2016).
[19] F.K.H. Gellersen, J. Peschel, A. Ochsenfarth, A.F. Jacob. 2017 Top. Work. Internet Sp., 1 (2017). https://doi.org/10.1109/TWIOS.2017.7869766
[20] S. Budiawanti, B. Soegijono, I. Mudzakir. AIP Conf. Proceed. **2023**, *1*, 20048 (2018).
[21] S.D. Yoon, C. Vittoria, S.A. Oliver. J. Appl. Phys. **93**, *7*, 4023 (2003).
[22] V.G. Kostishin, A.Yu. Mironovich, R.I. Shakirzyanov, I.M. Isaev, A.A. Sergienko. Usp. prikl. fiz. **8**, *5*, 370 (2020). (in Russian).
[23] B. Peng, J.Y. Jiang, W.L. Zhang, H.Z. Xu, W.X. Zhang. Mater. Res. Innov. **19**, *sup8*, S8-654 (2015).
[24] Q.F. Li, X.D. Su, H. Li, L. Zhang, Z.H. Liu, H.J. Zhong. J. Appl. Phys. **106**, *12*, 123914 (2009).
[25] C.V. Thompson, R. Carel. Mater. Sci. Eng. B **32**, *3*, 211 (1995).
[26] N.N. Shams, M. Matsumoto, A. Morisako. IEEE Trans. Magn. **40**, *4 Part 2,* 2955 (2004).
[27] A. Morisako, N.N. Shams, Y. Miura, M. Matsumoto, S.H. Gee, M.H. Park, Y.K. Hong. J. Magn. Magn. Mater. **272–276**, *Part 3,* 2191 (2004).
[28] A.R. Abuzir, S.A. Salman. Res. Phys. **8**, 587 (2018).
[29] Z. Xu, Z. Lan, K. Sun, Z. Yu, R. Guo, F. Bai. IEEE Trans. Magn. **49**, *7*, 4226 (2013).
[30] Y. Chen, J.A. Bain, M.H. Kryder. J. Magn. Soc. Japan. **21**, S_2_PMRC_97_2, S2_65 (1997).
[31] T.L. Hylton, M.A. Parker, M. Ullah, K.R. Coffey, R. Umphress, J.K. Howard. J. Appl. Phys. **75**, *10*, 5960 (1994).
[32] V.G. Kostishin, A.Yu. Mironovich, A.V. Timofeev, R.I. Shakirzyanov, I.M. Isaev, A.S. Kurochka, A.I. Ril', A.A. Sergienko. Russ. J. Inorg. Chem. **66**, *4*, 603 (2021).
[33] T. Guo, J. He, X. Pang, A.A. Volinsky, Y. Su, L. Qiao. Acta Materialia **138**, 1 (2017).
[34] G. Abadias, E. Chason, J. Keckes, M. Sebastiani, G.B. Thompson, E. Barthel, G.L. Doll, C.E. Murray, C.H. Stoessel, L. Martinu. J. Vac. Sci. Technol. A **36**, *2*, 020801 (2018).
[35] V.G. Kostishin, A.Y. Mironovich, A.V. Timofeev, R.I. Shakirzyanov, I.M. Isaev, G.A. Skorlupin, A.I. Ril. Mater. Today Commun. **31**, 103804 (2022).
[36] X. Zhang, S. Meng, D. Song, Y. Zhang, Z. Yue, V.G. Harris. Sci. Rep. **7**, *1*, 44193 (2017).
[37] T.S. Cho, S.J. Doh, J.H. Je, D.Y. Noh. J. Appl. Phys. **86**, *4*, 1958 (1999).

Translated by A.Akhtyamov